J Mater Sci: Mater Electron **(2023) 34:1792**

Design and fabrication of all-inorganic transport materials-based Cs_2SnI_6 perovskite solar cells

Dolly Kumari[1], Nilesh Jaiswal[2], Raghvendra Shukla[1], Deepak Punetha[3], Sushil Kumar Pandey[4], and Saurabh Kumar Pandey[1,*]

[1] *Sensors and Optoelectronics Research Group, Department of Electrical Engineering, Indian Institute of Technology Patna, Patna 801106, India*
[2] *Photonics Research Lab at School of Studies of Electronics and Photonics, Pt. Ravishankar Shukla University, Raipur, Chhattisgarh 492010, India*
[3] *Department of Electronics & Communication Engineering, Motilal Nehru National Institute of Technology Allahabad, Prayagraj 211004, India*
[4] *Department of Electronics and Communication Engineering, NIT Karnataka, Mangalore 575025, India*

Received: 23 May 2023
Accepted: 23 August 2023

ABSTRACT

With lead-based perovskite materials, lead content and long-term stability are the big concerns. Recently, Cesium tin iodide (Cs_2SnI_6) double perovskite has gained recognition as a stable and environment-friendly photovoltaic material compared to lead-based perovskite materials. In the present study, we have investigated Cs_2SnI_6 based solar cell with all inorganic transport materials using SCAPS-1D. The optimized device exhibited a maximum efficiency of about 18%. Further we fabricated Cs_2SnI_6 perovskite films using a solution process approach, utilizing CsI and SnI_4 in a 2:1 ratio. For synthesized double perovskite film, the crystallinity, morphologies, and optical characteristics were examined. Additionally, the stability analysis confirmed that the prepared perovskite films were stable for more than two months under ambient exposure. Finally, utilizing the synthesized Cs_2SnI_6 thin films as an absorber material, we fabricated two solar cells without and with hole transport layer (HTL), having configurations of glass/FTO/ZnO/Cs_2SnI_6/Ni and glass/FTO/ZnO/Cs_2SnI_6/ MoS_2/Ni, respectively, in the ambient conditions. As a major finding, it has been observed that the inclusion of MoS_2 as HTL improved overall performance, with an enhancement in the power conversion efficiency (PCE) of nearly 45% compared to the device without HTL.

1 Introduction

In recent years, climate changes brought up by the pollution demands for cleaner renewable energy technologies to meet the future requirements for energy [1]. The rising perovskite-based solar cells technique has drawn their attention from research communities because of its improved PCE that hikes from a value of 3.8% to about 25.7% in a very short amount of time [2]. Owing to the different electronic and optical behaviour

---

Address correspondence to E-mail: saurabh@iitp.ac.in

https://doi.org/10.1007/s10854-023-11197-w

of hybrid perovskite such as high carrier mobility, higher absorption coefficient, larger diffusion length, tunable bandgap and comparatively less costly fabrication technique make it more viable for photovoltaic application and drew much attention of the research communities [3–5]. Although hybrid perovskite has excellent qualities, the presence of lead is challenging because of environmental and ecological issues [6, 7]. In addition, the long-term stability due to the presence of organic cation is another significant issue related to this superior technology, preventing its massive application [8, 9]. To overcome the toxicity and stability issues, a number of research have been conducted for the advancement and development of lead-free perovskites that share many of the same properties as their lead-containing counterparts [6]. The Cs_2SnI_6 has distinguished itself as a leading material to replace lead-based perovskites among the possible lead-free options. The Cs_2SnI_6 possesses an optimal bandgap (Eg) in the range of 1.25–1.62 eV, absorption coefficient (over 10^5 cm^{-1}) and carrier mobility (1–509 cm^2 V^{-1} s^{-1}). In addition, Cs_2SnI_6 shows excellent stability in the air owing to the presence of Sn^{4+}. These properties make them a favourable choice for photovoltaic applications.

Qiu group was the first to utilize Cs_2SnI_6 as a light absorber material configured with c-TiO_2 and P3HT functioning as the electron transport layer (ETL) and hole transport layer (HTL), respectively. With an open-circuit voltage (Voc) of 0.51 V, the end design had an efficiency of 0.96% [10]. The same team later developed solar cell by diffusing the solution of Cs_2SnI_6 into the ZnO nanorod layer, resulting in a device efficiency of 0.86% [11]. Planar solar cell in a n-i-p configuration using the Cs_2SnI_6 perovskite was also employed, producing a PCE of 0.46% [12]. Further, spray-casted method was utilised to prepare Cs_2SnI_6 films. The prepared perovskite film was then assembled to develop perovskite solar cell (PSC) with the device architecture of FTO/CdS/ Cs_2SnI_6 /C/Ag. For PSC based on Cs_2SnI_6 and using CdS as the window layer, the fabricated device displayed the highest recorded Voc of 0.86 V [13]. Recently, Shodruz T. Umedov's group studied the effect of varying the A-site in Cs_2SnI_6, and they employed an inverted structure with the device configuration as ITO/CuI/Cs_2SnI_6-alloyed/PCBM/AZO/Ag, achieving a PCE of 0.135% with Cs_2SnI_6 and a PCE of 0.66% with alloyed films [14].

Despite numerous efforts and several synthesis processes reported so far [15–20], the device efficiency for Cs_2SnI_6 PSC is still relatively low. Together with synthesis and fabrication approaches, the choice of the ETL and HTL might also be very important for increasing device efficiency, as they can efficiently reduce the losses such as non-radiative recombination and current leakage. A desirable outcome can be obtained by combining the ETL, HTL, and the absorber/active layer in a balanced manner. Essentially, the ETL is the key component of a solar cell that separates the electrons from the absorber layer while block the holes to pass through it. Zinc oxide (ZnO) and Titanium dioxide (TiO_2) are suitable solar spectrum harvesting materials as ETLs. Of the two, ZnO is the most suitable candidate to be used as ETL, as it exhibits high electron mobility and has the advantage of being fabricated at a lower temperature [21]. HTL plays a significant role as well, as it blocks electrons and only permits holes to travel through it, much like ETL. Additionally, it serves the crucial purpose of isolating the moisture from stepping into contact with the perovskite absorber layer, which improves the stability of the device by lowering the possibility of degradation. Therefore, HTL must be selected carefully so that carrier transportation, device performance, and device stability can be improved [22, 23]. So far, the common hole transport materials (HTMs) exploited in standard PSC devices are organic ones, such as PEDOT:PSS, Spiro-OMeTAD, P3HT, etc. [24–26]. Although the PSCs utilizing organic HTMs exhibit excellent PCE, the main issue with these HTMs is their high manufacturing cost and at most, the stability issue affecting device performance. Employing inorganic HTMs could be suitable strategy to overcome the limitation found in organic HTMs. Several inorganic HTMs such as Cu_2O, CuO, Nio_x, CuI, CuSCN, MoO_x, MoS_2 has been utilised in PSCs, of which MoS2, a metal dichalcogenide having a direct bandgap of 1.2 eV, can be a suitable choice to be used as HTM owing to its better optical and electrical properties, solution processing ability, and thermal stability [27–29]. In recent years, MoS_2 has been used as the HTL in perovskite solar cells in a typical device configuration. It has also been used in inverted structures [30]. To utilise the MoS_2 as bulk HTL, its solubility is improved, or to obtain bulk HTM, the MoS_2 is spin coated for a few cycles. In addition, to increase efficiency and stability, a few layers of MoS_2 are coupled with Spiro-OMeTAD, an organic HTM [31]. Thus, utilising MoS_2 as HTL could be a reliable choice to enhance the cells' performance and reliability.

In this paper, we have carried out a simulation and experimental based study of Cs_2SnI_6-based solar cell with all inorganic transport materials, ZnO as the ETL and MoS_2 as the HTL. Two devices using Cs_2SnI_6 as an absorber material have been investigated without HTL and with HTL, having configurations as glass/FTO/ZnO/Cs_2SnI_6/Ni(device1) and glass/FTO/ZnO/Cs_2SnI_6/MoS_2/Ni(device2), respectively. For the synthesis of Cs_2SnI_6 double-perovskite film, a simple solution process approach has been followed [32], while the devices were fabricated using one step spin coating method. The fabricated devices exhibited an efficiency of 1.03% and 1.89% without and with MoS_2 layer, respectively. In addition to this, an exhaustive simulation has been performed which demonstrated that the proposed device performance can further improve upto 18% PCE subjected to a more sophisticated experimental environment, by optimizing the bulk defect.

2 Numerical modelling and experimental procedure

2.1 Simulation approach and device structure

Before carrying out the experimental work, we first investigated the proposed structure theoretically, since theoretical works offer a simple working environment to work with many facets of operation and analyze the key concerns. Theoretical works do not require any specific atmosphere, laboratory, or chemicals, but they do assist in selecting the optimal configuration and optimizing the various parameters so that the best performance of the PSCs may be obtained. This could not only save our time but also relieve us from the tedious job of continuously optimizing the different parameters such as thickness, defect density, doping density etc. while fabricating the device. As a result, trustworthy software programmes are required for leading the careful optimization of solar cells prior to fabrication. We designed and investigated all inorganic solar cell (device 1 and device 2) using solar cell capacitance (SCAPS-1D) software. Upto seven semiconducting layers can be used by the SCAPS-1D simulator for evaluating the different performance parameters of solar cells. It offers a platform where almost all factors, including charge carrier mobility, band-gap, electron affinity, and doping, may be changed in order to comprehend the physics of the device.

This tool utilizes Poisson equation (Eq. 1.), Continuity equations (shown by Eq. 2. and Eq. 3 for electron and holes, respectively) and drift–diffusion equations (shown by Eq. 4. and Eq. 5 for electron and holes, respectively) for modelling and estimating the device performance.

$$\frac{\partial}{\partial x}\left(\varepsilon\frac{\partial\Psi}{\partial x}\right) = -\frac{q}{\epsilon_0}\left[p - n + N_D^+ - N_A^- + \frac{1}{q}\rho_{defect}(n.p)\right] \quad (1)$$

$$-\frac{\partial j_n}{\partial x} + G - U_n(n,p) = \frac{\partial n}{\partial t} \quad (2)$$

$$-\frac{\partial j_p}{\partial x} + G - U_p(n,p) = \frac{\partial p}{\partial t} \quad (3)$$

$$j_n = qn\mu_n E + qD_n\frac{\partial n}{\partial x} \quad (4)$$

$$j_p = qn\mu_p E + qD_p\frac{\partial p}{\partial x} \quad (5)$$

where, n, p represents electron and hole concentration, N_D^+, N_A^- ionized donor and acceptor density,$\rho_{defect}(n.p)$ defect charge density, D_n, D_p electron and hole diffusion coefficients, U_n, U_p electron and hole recombination rates,G denotes generation rate, respectively.

All simulation work were carried out at 300 K. AM 1.5G with 100 WCm^{-2} constant illumination has been utilised for calculating performance parameters.

Figure 1(a) and (b) shows the the schematic structure and energy band diagram of proposed device, respectively. The simulation parameter values used for each layer for the theoretical investigation has been listed in Table 1. Values of different parameters were taken from the reported experimental and theoretical work [10, 11, 33, 34].

Here ε_r, E_G, χ, μ_n, μ_h, N_D, N_A, N_C and N_V represent relative permittivity, bandgap, electron affinity, mobility of electrons, mobility of holes, donor concentration, acceptor concentration, conduction band effective density of states, and valence band effective density of states, respectively.

2.2 Material details

All raw materials for fabrication purposes were purchased from Sigma Aldrich (USA) and used in similar form without further purification. The material that we used for fabricating device consist of cesium iodide

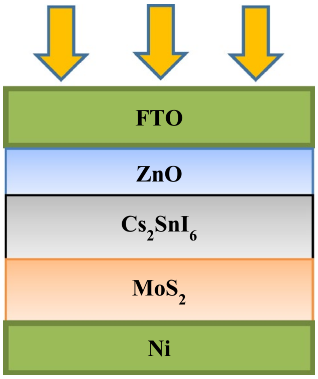

(a) Schematic structure of proposed

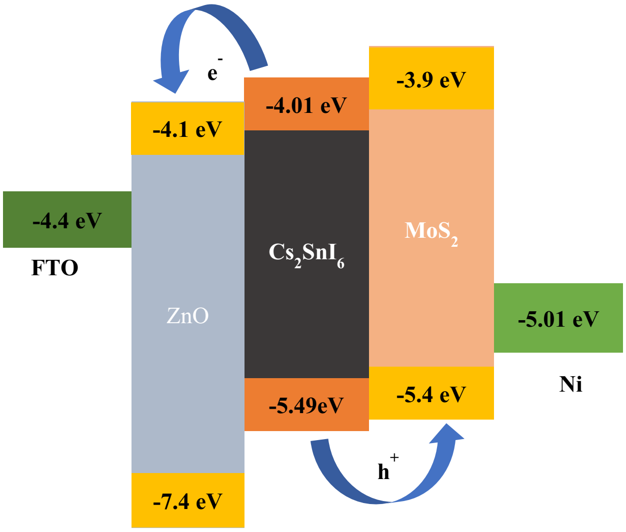

(b) Energy Band diagram of proposed device

Fig. 1 **a** Schematic structure of proposed device **b** Energy Band diagram of proposed device

Table 1 Simulation parameters used for theoretical investigation

Parameter	ZnO	Cs_2SnI_6	MoS_2
ε_r	9.0	10.0	13.6
E_G (eV)	3.27	1.48	1.29
χ (eV)	4.1	4.01	4.2
μ_n (cm^2/V. s)	100	0.38	100
μ_h (cm^2/V. s)	25	382	150
N_D (cm^{-3})	1.0×10^{18}	0	1.0×10^{15}
N_A (cm^{-3})	0	2.0×10^{15}	1.0×10^{17}
DOS(CB), Nc (cm^{-3})	2.2×10^{18}	2.2×10^{18}	2.2×10^{18}
DOS(VB), Nv (cm^{-3})	1.8×10^{19}	1.8×10^{19}	1.8×10^{19}

(CsI) anhydrous, beads (99.999%), tin (IV) iodide (SnI_4), anhydrous powder (99.999%), MoS_2 powder (99.99%), ZnO powder (99.9%).

2.3 Material synthesis

For the preparation of Cs_2SnI_6 solution, CsI and SnI_4 were dissolved in a 2:1 molar ratio in 3 ml of 2-isopropyl alcohol (IPA). After dissolving CsI and SnI_4 powders in the reaction solvent, they were then stirred gently for 3 h at room temperature (25 °C) and kept overnight, resulting in a double perovskite black solution at the end. The solution of MoS_2 has been prepared by dissolving 320.14 mg of MoS_2 powder in 2 ml of N-methyl-2-pyrrolidone (NMP) and stirring it for 2 h, while for the preparation of the ZnO solution, 814 mg of ZnO powder is dissolved in 10 ml of IPA, and the solution is stirred continuously for overnight at room temperature.

2.4 Device fabrication

We used fluorine-doped tin oxide (FTO) coated glass as a substrate for fabricating solar devices. The fabrication of thin films with uniform thickness frequently involves thermal vapor deposition system. However, because the precursor is uncontrolled, it is challenging to precisely regulate the composition of the film. Sol–gel is a low-cost chemical process that creates material by changing the liquid phase (sol) into the solid phase (gel) [35–38]. This form of fabrication typically involves a spin coating or dip coating process, followed by a heat treatment step. It has been discovered that annealing is essential to decrease material flaws. Annealing is a popular method used in the manufacturing of nanomaterials to either increase crystal quality or stabilize the structure at a temperature. In these tests, parameters like as annealing temperature and rotation speed were employed to study their impact on the creation of ETL, HTL, and perovskite. However, perovskite materials still have several drawbacks, such as deterioration due to water interaction and low thermal stability [39–41]. The temperature of perovskite thin films was optimized via a post-annealing process. First, FTO was cleaned in ultrasonic baths for 30 min each with DI water, acetone, and IPA. For the fabrication of devices, first, the ZnO sol–gel solution was spin-coated on the FTO substrate for 30 s at 3000 rpm. The as-deposited films were heated at 100 °C on a hot plate for 10 min. The prepared ZnO film was cooled down. The Cs_2SnI_6 solution was then spin-coated on prepared ZnO film for 50 s at 1000 rpm. In order to get uniform perovskite film and to evaporate the solvent part, we annealed the prepared perovskite film at 110 °C for 10 min. We repeated this process twice to obtain desired thickness for the absorber layer. Then, the MoS_2 solution was spin coated onto perovskite film at a rotation speed of 2000 rpm for 30 s. This was further followed by annealing the MoS_2 film at 150 °C on hot plate. After deposition of different layers, finally, the nickel (Ni) metal contact layer as a back electrode was deposited using the e-beam deposition method. Glass/FTO/ZnO/Cs_2SnI_6/Ni and glass/FTO/ZnO/Cs_2SnI_6/MoS_2/Ni, photovoltaic devices were fabricated following the above process under ambient conditions.

2.5 Characterization

Malvern Panalytical GIXRD with Cu-Kα 1.542 Å wavelength radiation, 2θ angle varying in the range of 10° to 60°, having tube voltage of 50 kV, and tube current of 100 mA was used to record the X-ray diffraction patterns, which were then used to analyse the structural characteristics of the deposited films. An ultraviolet–visible(UV–VIS) spectrophotometer (UV-2600 Shimadzu's proprietary model) was employed to calculate the UV–VIS absorption spectrum of Cs_2SnI_6. The surface morphology of Cs_2SnI_6 film has been investigated with field emission scanning electron microscope (FER-SEM; Zeiss Gemini SEM 500). A Keithley 2400 source meter was utilized for calculating the current density–voltage (J–V) characteristics. The performance parameters were calculated under AM 1.5 illumination with 100 mW/cm^2 produced by the Netport Oriel12A solar simulator. Across a 0.09 cm^2 active region, the J–V curves were measured.

3 Results and discussion

3.1 Simulation study of device 1 and device 2

ETL, HTL, and absorber layer thicknesses play an important role in deciding the performance of solar cells. For this, we first investigated the effect of the thickness of ZnO for both configurations, for which we varied the thickness of ZnO from 50 to 500 nm while keeping the thicknesses of other layers constant. It was found that with an increase in thickness from 50 nm to higher, the value of efficiency starts decreasing. Thus, the optimized thickness of ZnO was kept at 50 nm.

The absorber layer thickness significantly influences the PCE of PSCs hence, we varied it from 100 to 1500 nm. The value of Jsc increases with an increase in thickness for both devices. At a thickness of 100 nm, PCE of 6.12% with Voc of 0.6762 V was found, and after a thickness of 900 nm, a constant value of PCE of about 17% with a Voc of 0.9752 V was observed for device 1. Thus, optimized thickness of absorber layer for device 1 was kept as 900 nm. While for device 2, it was observed that at a thickness of 100 nm, a PCE of 7.93% with a Voc of 0.9251 V was found. An optimum efficiency of 18.18% was obtained at a thickness of 776 nm. Thus, the optimized thickness of the absorber layer for device 2 was kept at 776 nm. Figure 2 shows the PCE with the variation in the thickness of the absorber layer for both devices.

Keeping the thickness of absorber layer at 776 nm and ZnO at 50 nm for device 2, we varied the thickness of MoS_2 from 50 to 500 nm. The results showed a decrease in PCE as MoS_2 layer thickness varies from 50 to 500 nm. At a thickness of 50 nm MoS_2 layer, the maximum PCE was attained. Figure 3 shows effect on PCE of both devices with variation in ZnO and MoS_2 thicknesses.

3.2 Physiochemical properties

Crystallographic properties of the Cs_2SnI_6 perovskite thin film prepared using CsI and SnI_4 in a 2:1 ratio was examined from their X-ray diffraction patterns.

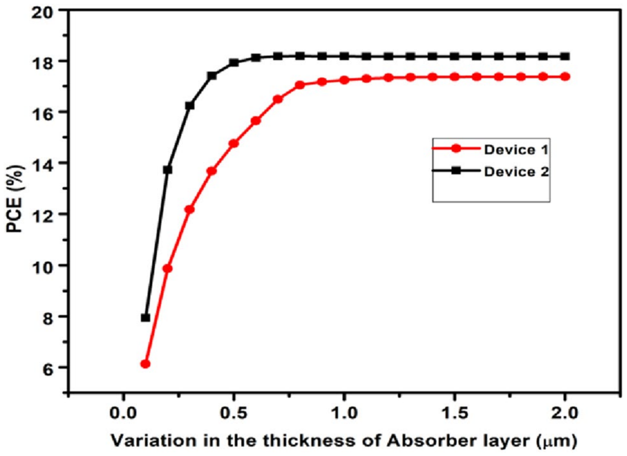

Fig. 2 Variation in the PCE with the variation in thickness of absorber layer

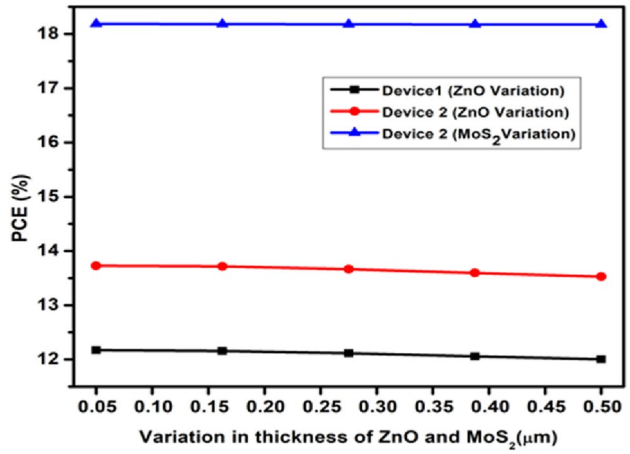

Fig. 3 Variation in the PCE with the variation in thickness of ZnO and Mos$_2$ layer

Figure 4 depicts the XRD pattern of Cs_2SnI_6 thin film deposited on FTO. From Fig. 1., we can observe that two major peaks are obtained at 2θ values equal to 26.5° and 30.7° that corresponds to atomic plane (222) and (004), respectively. Other peaks are obtained at 2θ values equal to 13.1°, 21.5°, 43.9°, 52.125° and 54.525°. These peaks correspond to atomic plane (111), (022), (044), (226), (444), respectively. The XRD peaks corresponding to atomic planes are identical to PDF# 73–0330 pattern and also is in good agreement with previously reported work [12, 13, 19, 32]. All obtained peaks were for Cs_2SnI_6 double perovskite. No peaks were observed for CSI which indicate the proper formation of perovskite material.

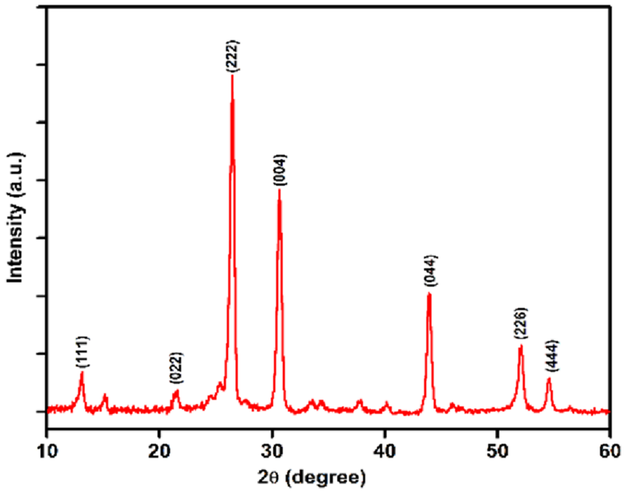

Fig. 4 XRD pattern of Cs_2SnI_6 thin film deposited on FTO

Figure 5 shows the Cs_2SnI_6 UV–VIS absorption spectra that was observed. The absorption band between 300 and 800 nm could be seen in the UV–VIS absorption spectrum. The obtained spectrum is in good agreement with previously published study [32].

The optimum performance of solar cell largely depends on the morphology of the absorber layer. For this, we examined the morphological characteristics of the Cs_2SnI_6 layer. Figure 6(a) and (b) shows the Cs_2SnI_6 FESEM images that were obtained (magnifications of 25 K at a scale bar of 1 µm) and cross-sectional image for the proposed Cs_2SnI_6 based solar cell. Compact and small crystals with clear edges having triangular and octahedral facets constitute the morphology.

3.3 Photovoltaic performance of fabricated devices

We fabricated two devices using Cs_2SnI_6 as light absorber material, in HTL and HTL-free configurations. J-V curves were used to evaluate the devices' performance. Figure 7 shows obtained J-V characteristics for the fabricated device. The obtained final performance parameters for the fabricated photovoltaic devices have been displayed in Table 2, along with the earlier notable works reported in this domain. It can be seen from Table 2 that the device without MoS_2 yielded PCE of 1.03%, V_{oc} of 0.436 V, a short circuit current density (J_{sc}) corresponding to 5.48 mA/cm^2, and fill factor (FF) of about 43.03%. While, with the incorporation of MoS_2 as the HTL, we obtained enhanced the efficiency. Its value rises from 1.03% to1.89% due to overall improvements in V_{oc}, J_{sc}, and FF. The improvement in performance parameters due to incorporation of the MoS_2 layer

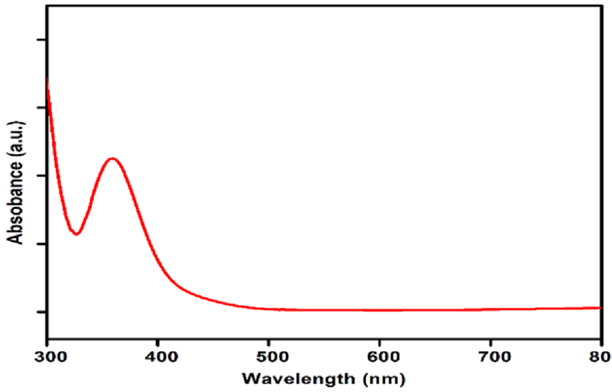

Fig. 5 UV–VIS absorption spectra of Cs_2SnI_6

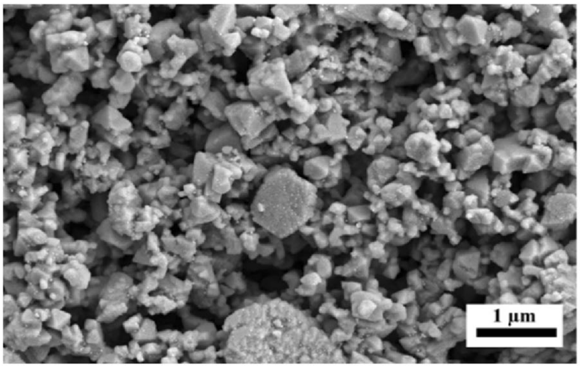

(a) FESEM image (top view) of Cs_2SnI_6 thin film at 25k

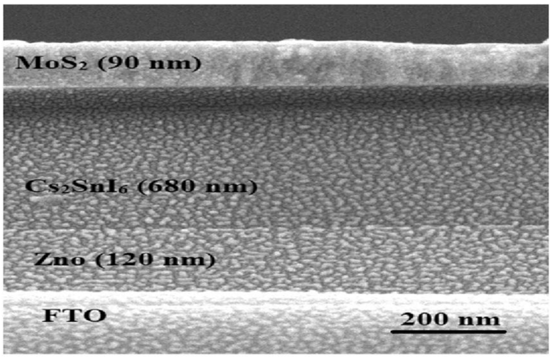

(b) Cross-sectional image for the proposed Cs_2SnI_6 based solar cell

Fig. 6 **a** FESEM image (top view) of Cs_2SnI_6 thin film at 25 k. **b** Cross-sectional image for the proposed Cs_2SnI_6 based solar cell

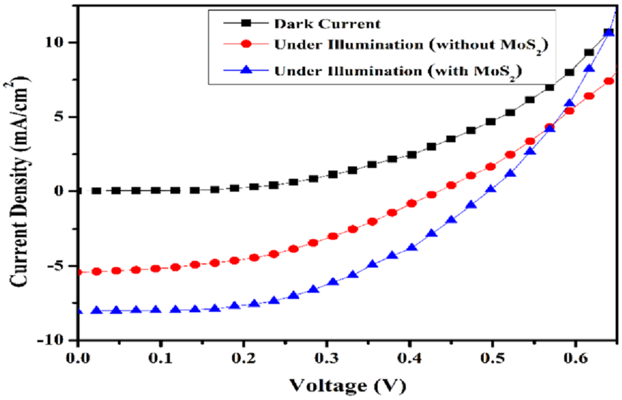

Fig. 7 J-V characteristics curve of Cs_2SnI_6 based fabricated device with and without MoS_2

can be explained from their energy band diagram as displayed in Fig. 1(b). In the absence of the MoS_2 layer, some of the photogenerated charge carriers travel to Ni electrode. This enhances the photocarrier recombination at the Cs_2SnI_6-Ni interface and thereby causes a reduction in the solar cells' current generation. While the MoS_2 layer raises its conduction band position significantly above that of Cs_2SnI_6, this prevents electrons from the absorber to pass through to the MoS_2 layer. The selective extraction of holes at the Cs_2SnI_6-MoS_2 interface reduces the recombination of the photogenerated carriers and hence improves the current generation of the solar cells. Thus, with the insertion of MoS_2 as HTL, the overall performance of the solar cell is enhanced.

3.4 Perovskite film and device stability

When we deal with perovskite materials, long-term stability is the major challenge since they degrade in the presence of moisture and oxygen. The produced Cs_2SnI_6 samples were stored at room temperature in ambient conditions to investigate their environmental stability. After 9 and 12 weeks, the prepared films were again examined using XRD, as shown in Fig. 8 (A-C). After 9 weeks a peak at 27.6° starts appearing. After 12 weeks the CSI impurity peak at 27.6° (JCPDS:77–2185) starts increasing. This shows that the film begins to degrade as a result of Cs_2SnI_6's disintegration in ambient conditions. Thus, prepared Cs_2SnI_6 film is stable for two months.

Furthermore, we also investigated device stability for which we took an unencapsulated Cs_2SnI_6 based solar cell (device 2) having initial PCE of 1.89%. The device 2 was kept under 1-sun illumination continuously for about 1000 min in an ambient environment. After 1000 min of continuous tracking, it was observed that device's PCE decreases only to 1.73%. Figure 9 shows the variation in PCE of device 2 with time. Thus, device 2 was able to preserves 91% of the initial PCE. after 1000 min, too.

3.5 Inconsistency of experimental result with the simulation analysis

In PSC, recombination plays a role in returning the non-equilibrium charge carriers generated by light back into a thermal equilibrium state. Recombination processes occur both within the bulk of the absorber material and at its interfaces, and they are generally undesirable. Commonly, defects in perovskite materials manifest as vacancies, while larger defects like grain boundaries and disruptions may also be present. The majority of defects in perovskite films are mostly observed on the surface or at the grain boundaries.

Table 2 Performance parameters of fabricated device and Comparative evaluation with Published Literature

S. No	Fabricated device Structure	J_{sc} (mA/cm^2)	V_{OC} (v)	FF (%)	PCE (%)	Ref
1	Glass/FTO/TiO_2/ Cs_2SnI_6/P3HT/Ag	5.41	0.51	0.35	0.96	[11]
2	FTO/TiO2/Cs2SnI6/P3HT/Ag	7.41	0.25	0.245	0.47	[12]
3	ITO/CuI /Cs2SnI6/PCBM/AZO/Ag	2.145	0.242	0.27	0.135	[13]
4	Glass/FTO/CdS/Cs_2SnI_6/C/Ag	0.33	0.86	0.37	0.11	[14]
5	FTO/TiO2/Cs_2SnI_6/Pt	6.752	0.367	0.595	1.47	[16]
6	**FTO/ZnO/Cs_2SnI_6/Ni**	**5.48**	**0.436**	**0.43**	**1.03**	**This work**
7	**FTO/ZnO/Cs_2SnI_6/MoS_2/Ni**	**8.11**	**0.498**	**0.4672**	**1.89**	**This work**

The bold represents, the results compiled for in this work

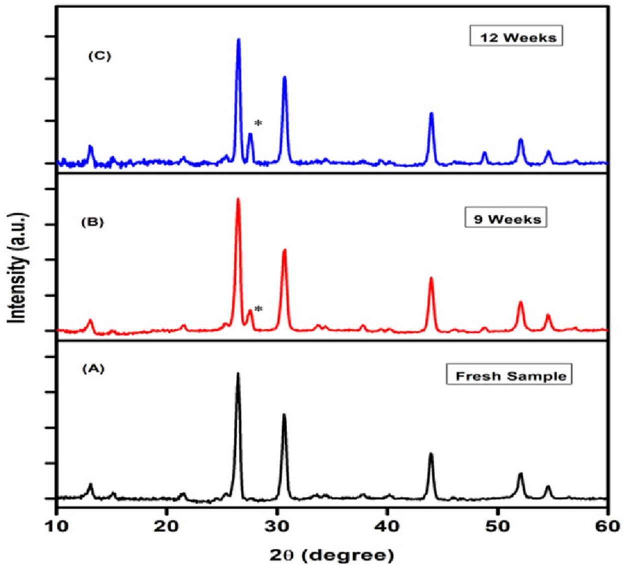

Fig. 8 XRD patterns obtained after 9 weeks and 12 weeks

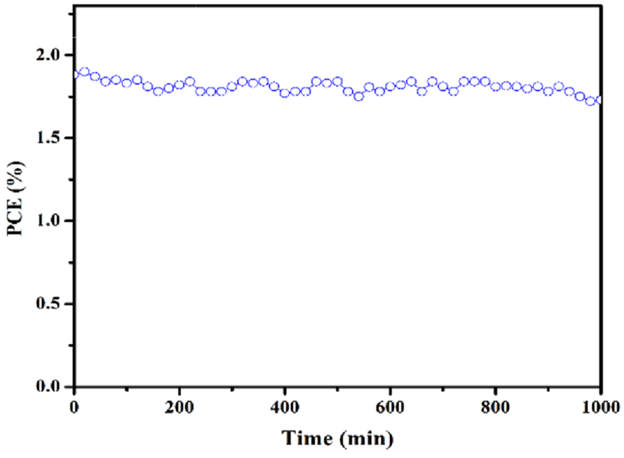

Fig. 9 Variation in PCE of device 2 with time

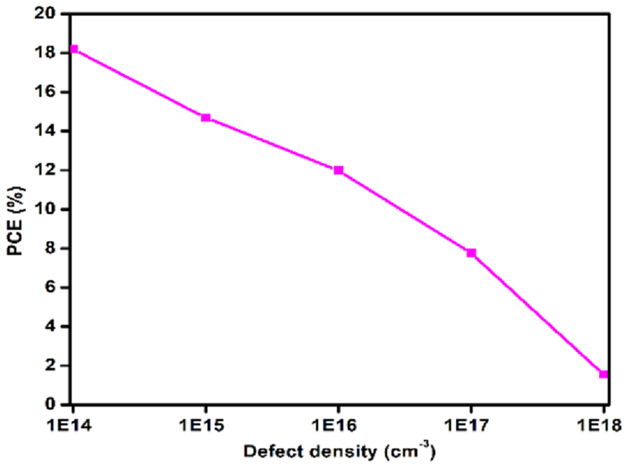

Fig. 10 Variation in PCE with bulk defect density

The density of these defect states is highly dependent on the film deposition procedures. These defects introduce shallow or deep energy levels within the bandgap. As a consequence of these imperfections, electrons and holes can become trapped, leading to the occurrence of the Shockley–Read–Hall recombination process [42]. Therefore, we need to concentrate on the techniques so that defect density can be reduced. This comprises the perovskite engineering so that the grain size can be enlarged, film morphology and crystallinity can be improved. Large grain size, smaller grain boundaries, and better crystallinity all contribute to a reduction in charge recombination, bulk defects, and surface defects in the perovskite films, which greatly enhances the device performance of perovskite solar cells.

To find a gap between experimental and theoretical efficiency, we tried to anticipate the proposed device behaviour at different bulk defects level ranging from 1×10^{14} cm^{-3} to 1×10^{18}, the corresponding variation is shown in Fig. 10. One can depicts from the figure that, the PCE significantly decreases from 18 to 2% as the level of defects get increased. Thus, rise in defects could be one of the probable reasons for the decrement of experimental efficiency [43]. In addition, while doing the experimentation, achieving the precise optimal thickness of the perovskite and transport layers is very challenging. The chemical processes involved during the fabrication of the perovskite layer can introduce slight variations in its thickness [44]. These variations can be attributed to factors such as the deposition technique, solution concentration, and reaction kinetics, which may affect the final thickness achieved. Therefore, achieving an exact and consistent thickness of the perovskite layer was difficult due to the inherent variability associated with the fabrication process. This may also lead to a lower experimental efficiency of the proposed PSC. Despite the inconsistency between the optimal numerical PCE and the experimentally achieved PCE for the proposed solar cells, it can be inferred that the device has the potential to exhibit excellent photovoltaic performance with the MoS_2 layer as a HTL and be subjected to fabrication in a more sophisticated environment.

4 Conclusion

In this work, we successfully synthesised and deposited air-stable Cs_2SnI_6 double perovskite films employing a one-step spin-coating technique. The successful synthesis of perovskite material is confirmed by the XRD spectrum. Further, we fabricated solar cells without and with HTL having configurations as glass/FTO/ZnO/Cs_2SnI_6/Ni and glass/FTO/ZnO/Cs_2SnI_6/MoS_2/Ni, respectively, using Cs_2SnI_6 films under ambient condition. Among the two devices, the device with HTL yielded optimum performance with Voc = 0.4672 V, Jsc = 8.11 mA/cm^2, FF = 46.72%, and PCE of 1.89%. In addition, as a conclusion, we found that the device with HTL exhibited an improved efficiency of around 1.89% compared to earlier reported results. The findings open a new path for developing an effective and stable Cs_2SnI_6 perovskite solar cell.

Acknowledgements

The authors express their deep gratitude to the Chemistry, Physics, and Mechanical departments of IIT Patna for accessing their resources for the characterization of prepared samples. The authors also express their gratitude to Prof. Marc Burgelman from the University of Ghent, Ghent, Belgium, for providing SCAPS-1D software to carry out research.

Authors contribution

Dolly Kumari: conception, methodology, simulation analysis, manuscript writing Nilesh Jaiswal: conception, methodology, formal analysis, manuscript writing Ragvendra Shukla: methodology, result analysis, proofreading Deepak Punetha: methodology, result analysis, proofreading Sushil Kumar Pandey: Continous supervision and proofreading Saurabh Kumar Pandey: Continous supervision and proofreading.

Data availability

Data sharing is not applicable.

Declarations

Competing interest The authors claim that they have no known conflicts of interest that would have affected the research findings in this study.

References

1. R. Wang, M. Mujahid, Y. Duan, Z.-K. Wang, J. Xue, Y. Yang, A review of perovskites solar cell stability. Adv. Func. Mater. (2019). https://doi.org/10.1002/adfm.201808843
2. National Renewable Energy Laboratory. Best Research-Cell Efficiency Chart (1976 to the present), (2020),https://www.nrel.gov/pv/cell-ffiEciency.html .
3. J. Huang, Y. Yuan, Y. Shao, Y. Yan, Understanding the physical properties of hybrid perovskites for photovoltaic applications. Nat. Rev. Mater. (2017). https://doi.org/10.1038/natrevmats.2017.42
4. P. Wang, Y. Wu, B. Cai, Q. Ma, X. Zheng, W.-H. Zhang, Solution-processable perovskite solar cells toward commercialization: progress and challenges. Adv. Funct. Mater. (2019). https://doi.org/10.1002/adfm.201807661

5. D. Kumari, S.K. Pandey, Comprehensive study and performance analysis of eco-friendly double perovskite Cs2AgBiBr 6 on Si tandem solar cell. J. Optical. Soc. AmericaB (2022). https://doi.org/10.1364/JOSAB.443938
6. B. Salhi, Y.S. Wudil, M.K. Hossain, A. Al-Ahmed, F.A. Al- Sulaiman, Review of recent developments and persistent challenges in stability of perovskite solar cells. Renew. Sustain. Ener. Rev. **90**, 210–222 (2018). https://doi.org/10.1016/j.rser.2018.03.058
7. D. Kumari, Saurabh Kumar Pandey, Effect of an ultra-thin 2D transport layer on eco-friendly Perovskite/CIGS tandem solar cell: A numerical study. Micro. Nanostruct. (2022). https://doi.org/10.1016/j.micrna.2022.207398
8. A. Babayigit, A. Ethirajan, M. Muller, B. Conings, Toxicity of organometal halide perovskite solar cells. NatMater **15**(3), 247–251 (2016). https://doi.org/10.1038/nmat4572
9. Ke. Weijun, M.G. Kanatzidis, Prospects for low-toxicity lead-free perovskite solar cells. Nat. Commun. (2019). https://doi.org/10.1038/s41467-019-8918-3
10. X. Qiu et al., From unstable CsSnI3 to air-stable Cs2SnI6: A lead-free perovskite solar cell light absorber with bandgap of 1.48eV and high absorption coefficient. Solar Ener. Mater. Solar. Cells (2017). https://doi.org/10.1016/j.solmat.2016.09.022
11. X. Qiu, Y. Jiang, H. Zhang, Z. Qiu, S. Yuan, P. Wang, B. Cao, Lead-free mesoscopic Cs_2SnI_6 perovskite solar cells using different nanostructured ZnO nanorods as electron transport layers. Phys. Status. Solidi. RRL **10**, 587–591 (2016). https://doi.org/10.1002/pssr.201600166
12. Y. Jiang, H. Zhang et al., The air and thermal stabilities of lead-free perovskite variant Cs_2SnI_6 powder. MaterialsLetters (2017). https://doi.org/10.1016/j.matlet.2017.04.046
13. A. Suazo, F. Josué, S. Shaji, D.A. Avellaneda, J.A. Martínez, B. Krishnan, Solar cell using spray casted Cs_2SnI_6 perovskite thin films on chemical bath deposited CdS yielding high open circuit voltage". SolarEnergy (2020). https://doi.org/10.1016/j.solener.2020.06.101
14. S.T. Umedov, D.B. Khadka, M. Yanagida, A. Grigorieva, Y. Shirai, A-site tailoring in the vacancy-ordered double perovskite semiconductor Cs_2SnI_6 for photovoltaic application. Sol. Energy Mater. Sol. Cells (2021). https://doi.org/10.1016/j.solmat.2021.111180
15. W. Zhu, T. Yao, J. Shen, W. Xu et al., In situ investigation of water interaction with lead-free all inorganic perovskite ($Cs_2SnI_xCl_{6-x}$)". J. Phys. Chem. C (2019). https://doi.org/10.1021/acs.jpcc.9b00720
16. B. Lee, C.C. Stoumpos, N. Zhou et al., Air-stable molecular semiconducting iodosalts for solar cell applications: Cs_2SnI_6 as a hole conductor. J. Am. Chem. Soc. **136**(43), 15379–15385 (2014). https://doi.org/10.1021/ja508464
17. J. Zhang, S. Li, P. Yang et al., Enhanced stability of lead-free perovskite heterojunction for photovoltaic applications. J MaterSci **53**, 4378–4386 (2018). https://doi.org/10.1007/s10853-017-1890-z
18. G. Kapil, T. Ohta, T. Koyanagi et al., Investigation of interfacial charge transfer in solution processed Cs2SnI6 thin films. J. Phys. Chem. C **121**(24), 13092–13100 (2017). https://doi.org/10.1021/acs.jpcc.7b04019
19. J. C.-R Ke., D. J. Lewis, A. S. Walton, B. F. Spencer, P. O'Brien, A. G. Thomas, & W. R. Flavell, Ambient-air-stable inorganic Cs2SnI6 double perovskite thin films via aerosol-assisted chemical vapour deposition. J. Mater. Chem. A **6**(24), 11205–11214 (2018). https://doi.org/10.1039/C8TA03133A
20. X.D. Wang, Y.H. Huang, J.F. Liao, Y. Jiang et al., In situ construction of a Cs_2SnI_6 perovskite nanocrystal/SnS_2 nanosheet heterojunction with boosted interfacial charge transfer. J. Am. Chem. Soc. (2019). https://doi.org/10.1021/jacs.9b04482
21. D. Liu, T. Kelly, Perovskite solar cells with a planar heterojunction structure prepared using room-temperature solution processing techniques. Nature Photon **8**, 133–138 (2014). https://doi.org/10.1038/nphoton.2013.342
22. J. Urieta-Mora, I. Garcia-Benito, A. Molina-Ontoria, N. Martin, Hole transporting materials for perovskite solar cells: a chemical approach. Chem Soc Rev. (2018). https://doi.org/10.1039/c8cs00262b
23. G.W. Kim, H. Choi, M. Kim, J. Lee, S.Y. Son, T. Park, Hole transport materials in conventional structural (n-i-p) perovskite solar cells: from past to the future. Adv Energy Mater (2020). https://doi.org/10.1002/aenm.201903403
24. Z. Hawash, L.K. Ono, Y.B. Qi, Recent advances in spiro-MeOTAD hole transport material and its applications in organic-inorganic halide perovskite solar cells. Adv. Mater. Interfaces. (2018). https://doi.org/10.1002/admi.201700623
25. D.Y. Liu, Y. Li, J.Y. Yuan, Q.M. Hong, G.Z. Shi, D.X. Yuan, J. Wei, C.C. Huang, J.X. Tang, M.K. Fung, Improved performance of inverted planar perovskite solar cells with F4-TCNQ doped PEDOT:PSS hole transport layers. J. Mater. Chem. A. (2017). https://doi.org/10.1039/C6TA10212C
26. Y. Zhang, M. Elawad, Z. Yu, X. Jiang, J. Lai, L. Sun, Enhanced performance of perovskite solar cells with P3HT hole-transporting materials via molecular p-type doping. RSC Adv. (2016). https://doi.org/10.1039/C6RA21775C
27. Md. Anower Hossain, B.A. Merzougui, F.H. Alharbi, N. Tabet, Electrochemical deposition of bulk MoS_2 thin films for photovoltaic applications. Solar Ener. Mater. Solar. Cells. (2018). https://doi.org/10.1016/j.solmat.2018.06.026

28. Y. Li, Y. Wang, Q. Zuo, B. Li, Y. Li, W. Cai, J. Qing, Y. Li, X. Liu, J. Shi, L. Hou, Improved efficiency of organic solar cell using MoS_2 doped poly(3,4-ethylenedioxythiophene) (PEDOT) as hole transport layer. Appl. Surf. Sci. (2022). https://doi.org/10.1016/j.apsusc.2022.153042
29. D. Wang, N.K. Elumalai, Md.A. Mahmud, H. Yi, M.B. Upama, R.A.L. Chin, G. Conibeer, C. Xu, F. Haque, L. Duan, A. Uddin, MoS_2 incorporated hybrid hole transport layer for high performance and stable perovskite solar cells. Synth. Metals. (2018). https://doi.org/10.1016/j.synthmet.2018.10.012
30. A. Capasso, F. Matteocci, L. Najafi, M. Prato, J. Buha, L. Cinà, V. Pellegrini, A.D. Carlo, F. Bonaccorso, Few-layer MoS2 flakes as active buffer layer for stable perovskite solar cells. Adv. Energy Mater. (2016). https://doi.org/10.1002/aenm.201600920
31. U. Dasgupta, S. Chatterjee, A.J. Pal, Thin-film formation of 2D MoS_2 and its application as a hole-transport layer in planar perovskite solar cells. Solar Energy Mater. Solar Cells **172**(2017), 353–360 (2017). https://doi.org/10.1016/j.solmat.2017.08.012
32. X. Nairui, T. Yehua, Q. Yali, L. Duoduo, W. Ke-Fan, One-step solution synthesis and stability study of inorganic perovskite semiconductor Cs_2SnI_6. Sol. Energy **204**, 429–439 (2020). https://doi.org/10.1016/j.solener.2020.04.079
33. D. Saikia, J. Bera, A. Betal, S. Sahu, Performance evaluation of an all inorganic $CsGeI_3$ based perovskite solar cell by numerical simulation. Opt. Mater. (2022). https://doi.org/10.1016/j.optmat.2021.111839
34. Md Dulal Haque, Md Hasan Ali, Md Ferdous Rahman, Abu Zafor Md Touhidul Islam, Numerical analysis for the efficiency enhancement of MoS_2 solar cell: A simulation approach by SCAPS-1D. Opt. Mater. (2022). https://doi.org/10.1016/j.optmat.2022.112678
35. H. Dixit, D. Punetha, S.K. Pandey, Performance investigation of Mott-insulator LaVO3 as a photovoltaic absorber material. J. Electron. Mater. (2019). https://doi.org/10.1007/s11664-019-07581-0
36. A. Kumar, N. Pandey, D. Punetha, R. Saha, S. Chakrabarti, Enhancement in the structural and optical properties after incorporation of reduced graphene oxide (rGO) nanocomposite in pristine CsSnBr 3 for solar cell application. ACS Appl. Electron. Mater. (2023). https://doi.org/10.1021/acsaelm.3c00224
37. A. Kumar, N. Pandey, D. Punetha, R. Saha, S. Chakrabarti, Tenability and improvement of the structural, electronic, and optical properties of lead-free CsSnCl3 perovskite by incorporating reduced graphene oxide (rGO) for optoelectronic applications. J. Mater. Chem. C **11**(10), 3606–3615 (2023). https://doi.org/10.1039/D2TC04586A
38. R. Shukla, D. Punetha, R. Kumar, S.K. Pandey, Examining the performance parameters of stable environment friendly perovskite solar cell. Optical. Mater. (2023). https://doi.org/10.1016/j.optmat.2023.114124
39. S. Ternes, J. Mohacsi, N. Lüdtke, H.M. Pham, M. Arslan, P. Scharfer, W. Schabel, B.S. Richards, U.W. Paetzold, Drying and coating of perovskite thin films: how to control the thin film morphology in scalable dynamic coating systems. ACS Appl. Mater. Interfaces. **14**(9), 11300–11312 (2022). https://doi.org/10.1021/acsami.1c22363
40. R. Shukla, R. Kumar, D. Punetha, S.K. Pandey, Design perspective, fabrication, and performance analysis of formamidinium tin halide perovskite solar cell. IEEE J. Photovoltaics. (2023). https://doi.org/10.1109/JPHOTOV.2023.3241793
41. P. Subudhi, D. Punetha, Progress, challenges, and perspectives on polymer substrates for emerging flexible solar cells: A holistic panoramic review. Prog. Photovoltaics: Res. Applications. (2023). https://doi.org/10.1002/pip.3703
42. R. Shukla, S. Pandey, Design, performance, and defect density analysis of efficient eco-friendly perovskite solar cell. IEEE Trans. Electron Devices (2020). https://doi.org/10.1109/TED.2020.2996570
43. B. Chen, H. Hu, T. Salim, Y.M. Lam, A facile method to evaluate the influence of trap densities on perovskite solar cell performance. J. Mater. Chem. C **7**, 5646–5651 (2019). https://doi.org/10.1039/C9TC00816K
44. M.F. Mohamad Noh, N.A. Arzaee, I.N. Nawas Mumthas, N.A. Mohamed, S.N.F. Mohd Nasir, J. Safaei, A. R. Bin M. Usoff, M. K. Nazeeruddin, and M. A. Mat Teridi, High-humidity processed perovskite solar cells. J. Mater. Chem. A **8**, 10481–10518 (2020). https://doi.org/10.1039/d0ta01178a